Investigation of the Effect of Magnetic Field on Mass Transfer Parameters of CO_2 Absorption Using Fe_3O_4-Water Nanofluid

Mohammad Hossein Karimi Darvanjooghi and Maedeh Pahlevaninezhad
Dept. of Chemical Engineering, Isfahan University of Technology, Isfahan, 84156-83111, Iran

Ali Abdollahi
Dept. of Mechanical Engineering, Najafabad Branch, Islamic Azad University, Najafabad, Iran

Seyyed Mohammadreza Davoodi
Dept. of Chemical Engineering, Isfahan University of Technology, Isfahan, 84156-83111, Iran

DOI 10.1002/aic.15571
Published online November 17, 2016 in Wiley Online Library (wileyonlinelibrary.com)

In this study, the enhancement of physical absorption of carbon dioxide by Fe_3O_4-water nanofluid under the influence of AC and DC magnetic fields was investigated. Furthermore, a gas-liquid mass transfer model for single bubble systems was applied to predict mass transfer parameters. The coated Fe_3O_4 nanoparticles were prepared using co-percipitation method. The results from characterization indicated that the nanoparticles surfaces were covered with hydroxyl groups and nanoparticles diameter were 10–13 nm. The findings showed that the mass transfer rate and solubility of carbon dioxide in magnetic nanofluid increased with an increase in the magnetic field strength. Results indicated that the enhancement of carbon dioxide solubility and average molar flux gas into liquid phase, particularly in the case of AC magnetic field. Moreover, results demonstrated that mass diffusivity of CO_2 in nanofluid and renewal surface factor increased when the intensity of the field increased and consequently diffusion layer thickness decreased. © 2016 American Institute of Chemical Engineers *AIChE J*, 63: 2176–2186, 2017
Keywords: magnetic field, CO_2 absorption, nanofluid, Fe_3O_4 nanoparticles

Introduction

To date, the synthesis of Iron-oxide as a supermagnetic nanoparticles has been intensively developed for its many interesting properties leading to many important applications in almost all the fields ranging from ferrofluids, catalyst, magnetic recording media, solar energy transformation to medical application, and therapeutic agents for cancer treatment.[1] These applications demand chemically stable and uniformly sized nanoparticles with specific surface characteristics and magnetic properties that can be well dispersed in aqueous media. Among magnetic iron oxides, magnetite is a very promising choice for industrial and biological applications. To understand the Ferrofields' behavior, the liquid's location can be manipulated under the influence of an applied field, and careful studies related to fluid stability, particle sizes, and control of surfactant are essential.[2–4] For the synthetic method of magnetite nanoparticles, many different methods have been developed to prepare Fe_3O_4 based on the process media including gas phase methods, such as chemical vapor deposition,[5] microwave-assisted,[6] laser pyrolysis,[7] reduction of hematite CO/CO_2 or Hydrogen,[8] and liquid phase methods, such as the chemical co-precipitation,[9] microemulsion,[10,11] sol-gel,[12,13] and ball milling carried out in the solid phase.[7,14] Among these methods, liquid phase probably offers the most promising process control, scalability, superior yields of products as well as convenient for surface treatment. As a consequence, most nanoparticles have been produced via co-precipitation technique from aqueous solutions.[15] Ferrofluids were first developed in the 1960s by Pappell for high-performance seals in space applications and they are currently employed for the same purpose in various machines, ranging from computer discs unit to centrifuges.[3] Fe_3O_4 nanoparticles, due to the large surface-area to volume ratio, have tendency to aggregate in solution to reduce their surface energy; therefore, these inherent unstable particles should be stabilized by adding dispersing agents in the suspension and applying ultra-sonication treatment to minimize particle aggregation in the base fluids. In recent advanced nanoparticle synthesis, Berger et al. prepared aqueous-metal-based ferrofluid based on reacting iron (II) and iron (III) ions in an aqueous ammonia solution to form magnetite, Fe_3O_4. Moreover, the colloidal stability of the suspension was achieved by coating the particle surface with tetramethylammonium hydroxide.[3] Cheng et al. synthesized non-polymer coated Fe_3O_4 nanoparticles using Fe (II) and Fe (III) salt in the presence of tetramethylammonium hydroxide to form chemical precipitation.[16] Following this work, Andrade et al. obtained nanopaticles of magnetite by reacting sodium sulphite with ferric chloride, through the reduction-precipitation method. They alkalinized the iron oxide with tetramethylammunium hydroxide and ammonia and indicated that cations of surfactant adsorbed onto the surface of the synthesized nanoparticles gave rise to repulsive stabilization forces that led to more colloidal stability of particles and the enhancement of the transformation of the amorphous material.[17] Que et al. developed a method

Correspondence concerning this article should be addressed to M. H. Karimi Darvanjooghi at mh.karimi@ce.iut.ac.ir or mohamadkarimi1369@yahoo.com.

to prepare spherically-shaped magnetite nanoparticles smaller than 10 nm by partial reduction of ferric ions with Na_2SO_3 before adding the precipitation agent.[18] Angela et al. investigated the effect of the pH on the chemical properties of the synthesized magnetite nanoparticles. They investigated magnetic properties of the formed nanoparticles in detail and reported that with the final pH between 9.7 and 10.6 pure magnetite was produced.[19]

Application of novel techniques using various fluids on mass transfer rate[20] and the use of nanoparticles in fluids was also proposed for enhancement of mass transfer process.[20,21] H_2S and CO_2 removal from biogas and the study of the presence of nanoparticles in water to enhance mass transfer in conventional techniques based on physical absorption has received more attention in recent years. Xuan et al. investigated mass transfer in nanofluids and developed a mathematical model to estimate the mass transfer rate in nanofluid.[22] They suggested a method for finding the mass diffusion coefficient and the mass transfer coefficient by means of the heat and mass transfer analogy. Moreover, they showed that the microconvection enhanced the mass transport process by establishing a complicated theory. Esmaeili Faraj et al. investigated the effects of exfoliated graphene oxide nanosheets dispersed in water on mass transfer and showed that the mass transfer rate of hydrogen sulfide increased up to about 40%. They also investigated the absorption of carbon dioxide and hydrogen sulfide using exfoliated graphene oxide in water and synthesized silica-water nanofluids in a bubble column. They observed that the adsorption increased more than 500 and 200% due to oxygen group functionalities and silanol groups.[23] They showed that particles with high adsorbing capacity can circulate between the diffusion gas-rich layer near to the interface where adsorption takes place, and the bulk where desorption occurs,[23,24] and speculated that grazing was the main reason for the enhancement of mass transfer in EGO-water nanofluids.

In this study, coated Fe_3O_4-water nanofluid was synthesized to investigate the mass transfer enhancement of CO_2 absorption and study the effectiveness of nanoparticles and magnetic fields on the absorption parameters (diffusivity, diffusion layer thickness, renewal surface factor, and concentration of CO_2 at bubble-nanofluid interface) using a bubble column absorber. To generate nearly uniform magnetic fields in a vertical direction (parallel to bubble flow), AC and DC voltages were applied to the solenoid coil with maximum intensity of 720 gausses. A co-precipitation method was used to prepare the magnetic nanoparticles. Dynamic light scattering (DLS), transmission electron microcopy (TEM) analysis, Zeta potential measurement, Fourier Transform Infrared Spectroscopy, and X-ray diffraction (XRD) tests were applied to characterize the nanoparticles.

Experimental Apparatus and Procedure

Materials

For ferrofluid synthesis, ferric chloride hexahydrate ($FeCl_3.6H_2O \geq 97\%$), ferrous chloride tetrahydrate ($FeCl_2.3H_2O \geq 99\%$), HCl and ammonia solution (25 wt %) were obtained from Merck Company. A surfactant tetramethylammonium hydroxide, $(CH_3)_4NOH$ (TMAH), was also purchased from Merck Company. Deionized water was used as a solvent for washing glassware and preparing nanofluid with various concentrations. Strong permanent magnet was used for precipitating the Fe_3O_4 nanoparticles with maximum magnetic intensity of 1200 gausses, purchased from All Magnetics Incorporation Company.

Instruments

In this study, analytical techniques, such as TEM and DLS were applied to measure size distribution of magnetic nanoparticles. The TEM images of Fe_3O_4 nanoparticles were recorded using Hitachi, 9000 NA, Japan to characterize the particle sizes and the extent of agglomeration.[17] To prepare the sample used in TEM, an extremely little amount of the suspension of the nanoparticle dispersed in water was sonicated, (Ultrasonic bath, Parsonic 30S-400W, 28 kHz), for 20 min and was placed on the 400 mesh copper grid. Then, the grid was put in an evacuated desiccator to evaporate the solvent before being introduced into the microscope. DLS, Malvern, ZetaSizer Nano ZS, was applied to determine the agglomerate grain sizes and observe the size distribution of the obtained magnetite nanoparticles in suspension.[17,19,23] The zeta potential was determined using Malvern, ZetaSizer Nano ZS, to measure nanofluid stability. The ATR-FTIR data were obtained with a FT-IR model Tensor 27 Bruker to investigate the chemical structure of the magnetite nanoparticles. The precipitated magnetite nanoparticles were characterized by XRD, Bruker, to estimate structure of synthesized iron oxide at room temperature. A pH meter (PCE-PHD 1) with a memory recorder was used for recording pH of solutions vs. time.

Nanofluid preparation

In this study, Fe_3O_4 nanoparticles were synthesized based on co-precipitation method similar to the one described in literature.[25] In first step, 60 mL of 2M HCl solution were prepared by dissolving 10 mL of 12M HCl and 50 mL of distilled water. Then, a solution of ferric chloride hexahydrate (3.976 g, solution I) in 12M HCl (10 mL) and a solution of ferrous chloride tetrahydrate (13.515 g, solution II) in 12M HCl (50 mL) were prepared and the resulting mixture of solution I and II in the volume ratio 1:4 were stirred for 10 min in a flask. After mixing 4.0 mL of $FeCl_2.4H_2O$ and 2.0 mL of 1M $FeCl_3.6H_2O$, to oxidize the iron ions and form precipitate, 13.2 mL of a NH_4OH stock solution containing 25 wt % was diluted to a total volume of 250 mL and 50 mL of diluted NH_4OH (50 mL of 1M NH_4OH solution) was added by means of a syringe pump set on a 250 mL /h flow rate under vigorous stirring. The reaction in this stage took place as follow using NH_4OH solution:

$$2Fe^{3+} + Fe^{2+} + 4OH^- \rightarrow Fe_3O_4 + 4H^+ \quad (1)$$

The pH of the reactants was monitored during precipitation until the pH was increased to approximately 12. The color change in the solution from orange to dark-black was characteristic of magnetite synthesis. The suspension of precipitated powder was stirred at 1200 rpm for 20 min and to separate the magnetite, strong permanent magnet was hold beneath the boat and the precipitates were given a wash by means of deionized water and centrifuged at 2000 rpm for 5 min. Finally, after discarding the supernatant from precipitate, 8 mL of TMAH stock solution containing 25 wt % was added to centrifuge tubes containing nanoparticles at 25°C under stirring (450 rpm) for 30 min. To prepare ferrofluid, the precipitate was again centrifuged in TMAH medium at 15,000 rpm for 15 min. The ferrofluid was prepared with mechanical dispersing of coated Fe_3O_4 nanoparticles in distillated water to obtain suspensions with nanoparticle concentrations of 0.005, 0.01, 0.05, 0.1, 0.5, 1, 2, and 4 wt %. The obtained samples before adding surfactant were black in color and they also exhibited magnetic behavior, as it was

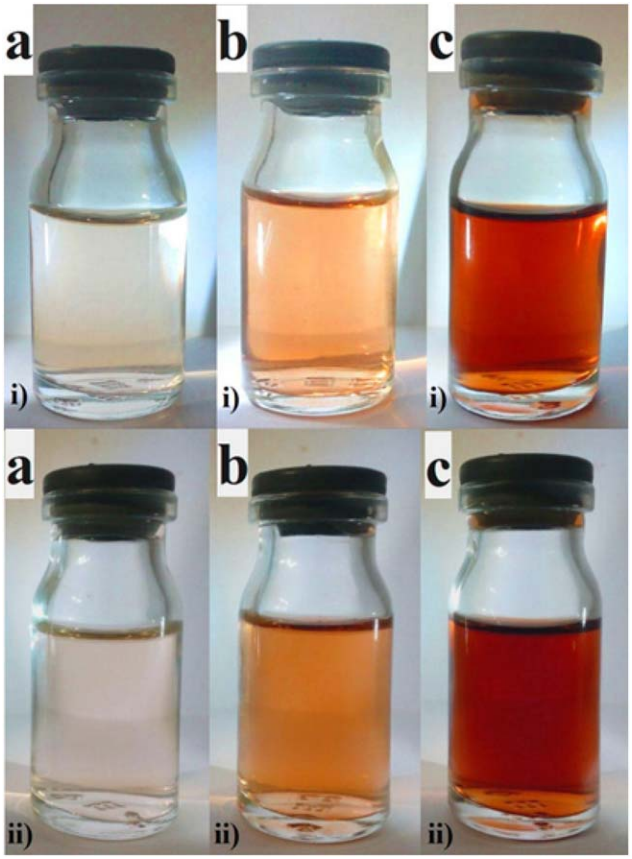

Figure 1. Image of Fe_3O_4-water nanofluid (i) quickly after synthesis and (ii) two months after synthesis for mass fractions of (a) 0.005, (b) 0.01, and (c) 0.1 wt %.

[Color figure can be viewed at wileyonlinelibrary.com]

exposed to the magnetic field of a permanent magnet. Centrifuging the sample in aqueous suspension in absence of TMAH at 2000 rpm for 5 min separated precipitates from aqueous solution, but in the case of precipitate centrifuged in TMAH, centrifugation even at 15,000 rpm took more than 10 min to separate them from the liquid phase suggesting that these particles were more stable. After centrifugation of nanoparticles and separating TMAH from suspension, three various nanofluids with mass fractions of 0.005, 0.01, and 0.1 wt % were prepared using dispersing remained nanoparticles in deionized water. The images of nanofluids with different concentrations are shown in Figure 1. These images show that there was no significant aggregation and precipitation of nanoparticles in the samples that substantiated the stability of nanoparticles in the basefluid, optically.

Experimental procedure

The analysis for carbon dioxide absorbed in the liquid phase involves a reverse titration using a pH meter and a standard HCl solution. According to method of reverse titration, to determine carbon dioxide content by titration, it is required to convert the carbonic acid to the carbonate ion by the addition of strong standard base. In this study; column content was discharged to the flask containing 15 mL of 0.1 M NaOH solution. The carbon dioxide in the solution reacted with the sodium hydroxide and formed sodium bicarbonate as below[23]:

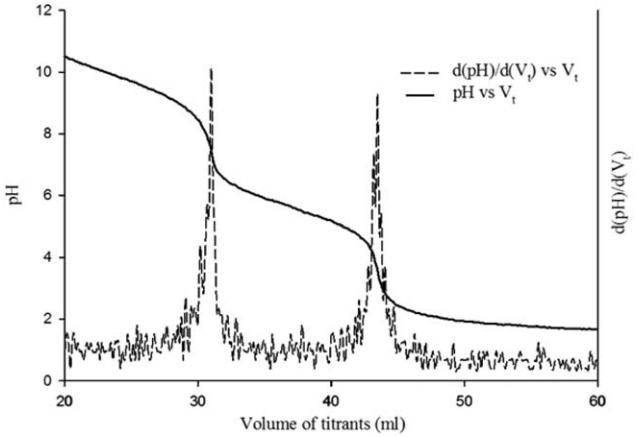

Figure 2. Titration curve for the base fluid containing 1 wt % TMAH after CO_2 absorption.

$$CO_2 + 2NaOH \rightarrow Na_2CO_3 + H_2O \quad (2)$$

Then, a titration was performed to determine the amount of NaOH in excess and excess HCl (as a titrant) in the flask reacted with Na_2CO_3 during the titration as Eqs. 3 and 4:

$$Na_2CO_3 + HCl \rightarrow NaCl + NaHCO_3 \quad (3)$$

$$NaHCO_3 + HCl \rightarrow NaCl + H_2O + CO_2 \quad (4)$$

According to Eq. 3, the sample was titrated with standard acid to pH 8.4 (first equivalent point which any excess hydroxide ions were neutralized and the carbonate ions converted to bicarbonate). Further titration to pH 4.0 with HCl converted all the bicarbonate to carbon dioxide and carbonic acid (Eq. 4). In this technique, the difference of consumed HCl between two equivalent points represents the amount of carbon dioxide in the solution as Eq. 5.

$$C_{CO_2} = \frac{(V_2 - V_1) \times M}{V} \times 10^3 \quad (5)$$

Where C_{CO_2} is the absorbed CO_2 concentration in the nanofluid (mol/m^3), M is HCl concentration (mol/L), and V is liquid volume in the absorber column equal to 100 mL in all experiments. V_1 and V_2 are the volume (mL) of HCl solution consumed for first and second equivalent points, respectively (Figures 2 and 3).

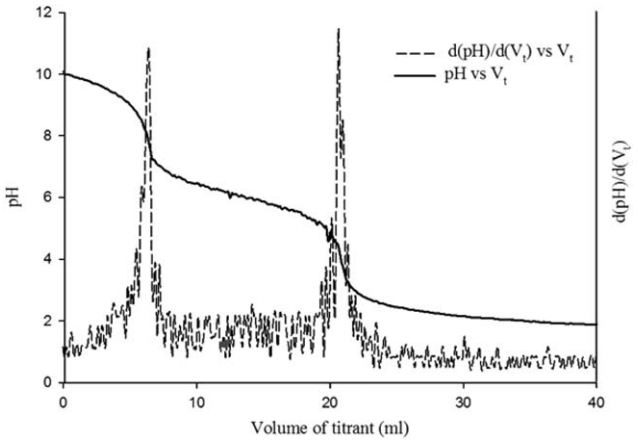

Figure 3. Titration curve for the nanofluid containing 1 wt % coated Fe_3O_4 nanoparticles after CO_2 absorption.

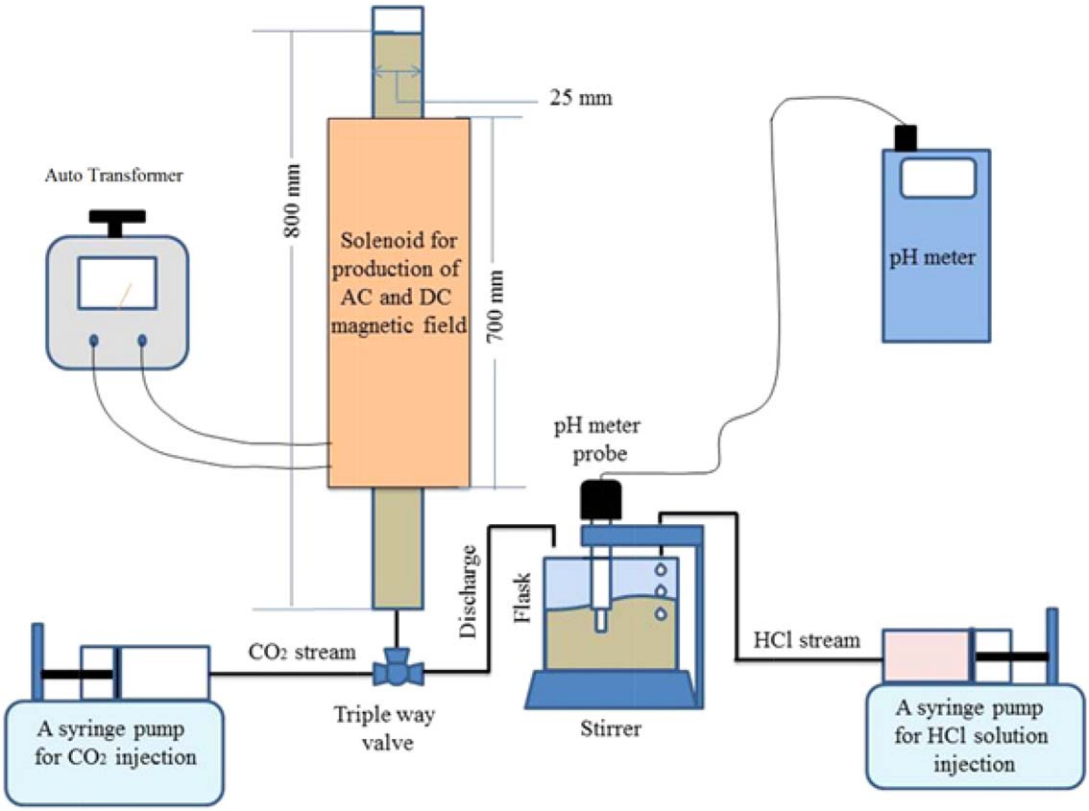

Figure 4. A schematic representation of experimental set-up used for the examination of the effectiveness of nanoparticles and magnetic fields on the absorption parameters.

[Color figure can be viewed at wileyonlinelibrary.com]

In this experiment, the molar flux of absorbed carbon dioxide can be calculated by means of the carbon dioxide concentration in the nanofluid (Eq. 6):

$$N_{av} = \frac{C_{CO_2} \times V}{n \times 4\pi r_0^2 \times \theta} \times 10^{-6} \quad (6)$$

Here, N_{av} is the average molar flux transferred from gas to liquid (mol/m^2 s), n is the number of single bubbles injected into the column, θ is total gas liquid contact time of one single bubble with the liquid (s) measured by multiplying rising time of one bubble through nanofluid to the number of bubbles, and r_0 is bubble radius which it was constant (m).

The set of experiments were applied to obtain mass transfer parameters such as diffusion coefficient and liquid mass transfer coefficient. In the first step, CO_2 was injected at the bottom of the column and rose along the nanofluid within volumes of 25, 30, 35, 40, 45, 50, 55, and 60 mL. Then, mass transfer parameters was determined using measuring the absorption of CO_2 in the presence of magnetic field and regression analysis of the mathematical model suggested by zhao et al.[26] Afterward, this theoretical conclusion was validated by comparing them with the data obtained from experimentations. Finally, estimated mass transfer parameters such as mass diffusivity was compared with values obtained from a correlation suggested in other literate.[27] Temperature of column content, as a key factor that affected the absorption of CO_2, was measured at the beginning and at the end of each test. Since the gap between the solenoid and bubble column was less than 2 mm adding cooling system was not applicable and also due to the large diameter of bubble column respect to outer surface this causes temperature gradient during applying magnetic field. To make sure that the solenoid and the bubble column were at room temperature (25°C), the time of each test was limited to 30 s attempt with a cool-down period of 1.5 min between each attempt until whole amount of CO_2 was injected to the nanofluid. Experimental data showed that it took about 1 min for nanofluids in a bubble column when exposed to magnetic field with magnitude of 720 G for 30 s to cool down to ambient temperature; therefore, 1.5 min total elapsed time before any further attempts were made. To check whether it caused errors or not, samples were titrated immediately after absorption and 30 min after each completed test, (the vessel containing nanofluid after each experiment was capped to prevent CO_2 desorption during 30 min). The carbon dioxide contents were same for both situations declaring no desorption was occurred during cooling time attempts.

Experimental apparatus

In general, the experimental set-up consisted of a bubble column absorber that was exposed to a parallel direct (unidirection) and alternating current magnetic fields and specific volume of carbon dioxide was injected to nanofluid within the absorption column. A solenoid which had a maximum intensity of 720 gausses was used to apply AC and DC magnetic fields. Figure 4 shows the schematic view of polyethylene bubble column with 800 mm high and 25 mm diameter used as a semi-continuous instrument to study gas absorption. Moreover, the solenoid was 70 cm long and consisted of 9540 turns of insulated wire wound and it appeared from results that a direct and alternating currents of 2 and 2.5 A, respectively, sent through the solenoid created electromagnetic fields of intensity 720 gausses. A deiod bridge (ZOUGUANG/SUNIZ,

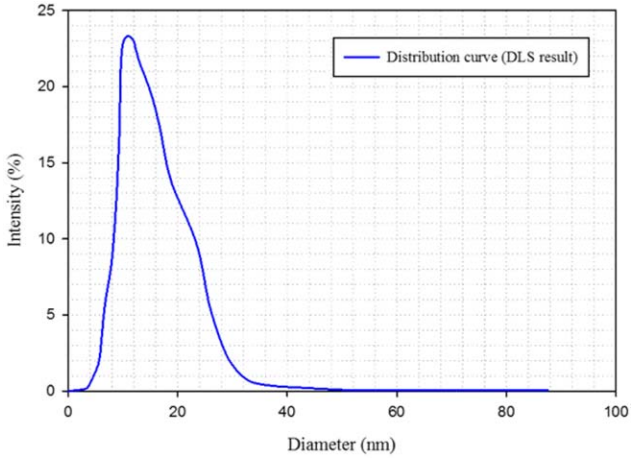

Figure 5. Dynamic light scattering (DLS), distribution curve of coated-Fe_3O_4 nanoparticles vs. particle size diameter.

[Color figure can be viewed at wileyonlinelibrary.com]

China) was applied to convert alternating current (pulsed electricity runs on 50 Hz) into direct current (a continuous current), and to maintain a constant voltage level and vary the output voltage as per our requirement, an autotransformer (TDGC2, Winston) was applied. A digital scale model CBB-50, Contech Instruments Ltd, India, was used for measuring chemical materials weights. A syringe-pump (Viltechmeda, Plus SEP21S) was applied for injection of CO_2 through the absorber column and injection of HCl solution to discharged nanofluid. Also a magnetic stirrer Model IKA-10038, Germany was used for stirring the solutions.

Uncertainty analysis

In this work, the uncertainty of the final experimental results was determined by the measurements errors of the parameters, including time, liquid volume, and pH of solutions. In the experimental investigation, time was measured by a digital chronometer, the pH of solutions by a pH meter, and the liquid volumes with laboratories glassware. The uncertainty of final experimental results was obtained as follow[28,29]:

$$U = \pm\sqrt{\left(\frac{\Delta V}{V}\right)^2 + \left(\frac{\Delta t}{t}\right)^2 + \left(\frac{\Delta \mathrm{pH}}{\mathrm{pH}}\right)^2} \tag{7}$$

The accuracy of pH meter, digital chronometer, and laboratories glasswares were ± 0.1, ± 0.01 s, and ± 0.1 mL, respectively. Consequently, the uncertainty of the experimental results was approximately less than 6.3%.

Results and Discussion

Nanofluid characterization

According to Figure 5, DLS analysis of dispersed Fe_3O_4 nanoparticles in water shows that the mean nanoparticle diameter is found to be 11 nm. This result confirms that the synthesis technique led to the well dispersed particles, mostly in the range of 11 to 13 nm.

Figure 6 shows the TEM images of magnetic nanoparticles synthesized via co-percipitation method. It shows that the average diameter of coated-Fe_3O_4 nanoparticles were 11 nm. These results are in consistent with those of DLS analysis. Moreover, Figure 7 represents the semi-spherical morphology of nanopraticles that the agglomeration was not occurred.[30]

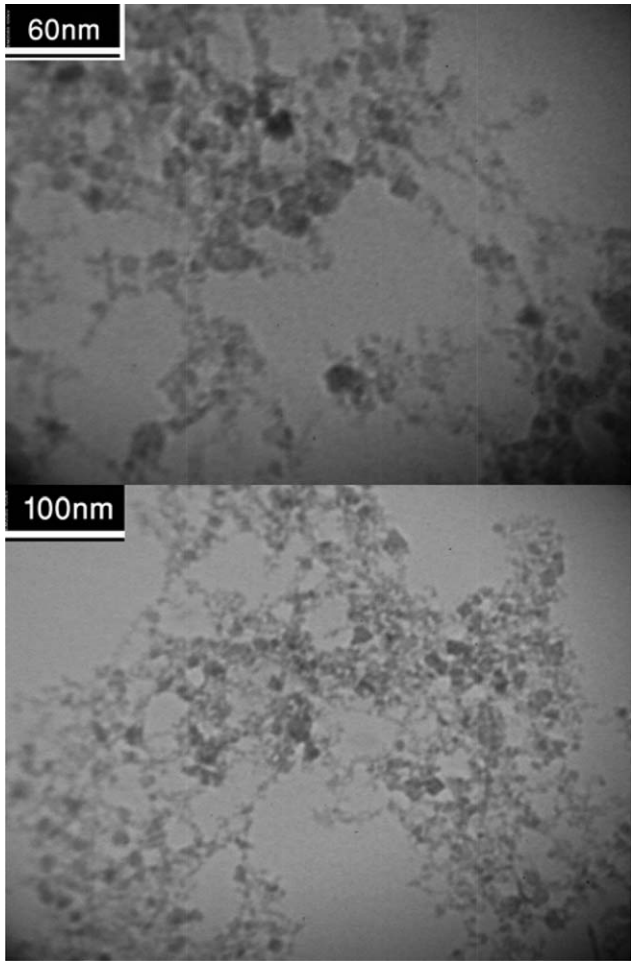

Figure 6. TEM image of coated-Fe_3O_4 nanoparticles.

Figure 7 shows the result of zeta potential analysis and it confirms that nanofluid has high stability.[31] The Zeta potential is a key indicator of the stability of nanoparticles.[32] In other words, the magnitude of the zeta potential determines the degree of electrostatic repulsion between similarly charged particles in colloidal dispersions. According to Figure 7 the large magnitude of the zeta potential (-58.8 to -39.9 mV) indicated stability of nanoparticles that did not tend to agglomerate due to repulsive electrostatic forces.[33]

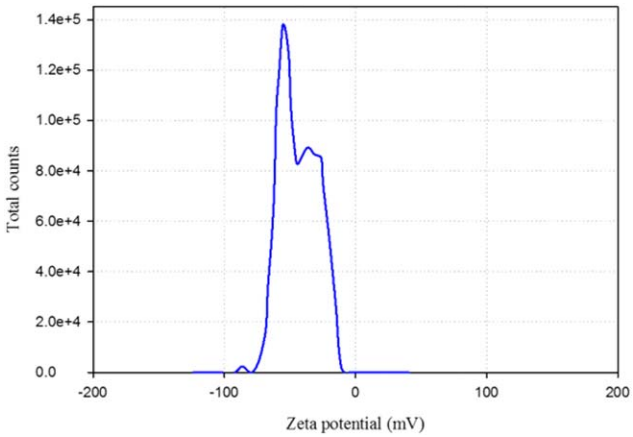

Figure 7. Zeta potential diagram for coated Fe_3O_4/water nanofluid.

[Color figure can be viewed at wileyonlinelibrary.com]

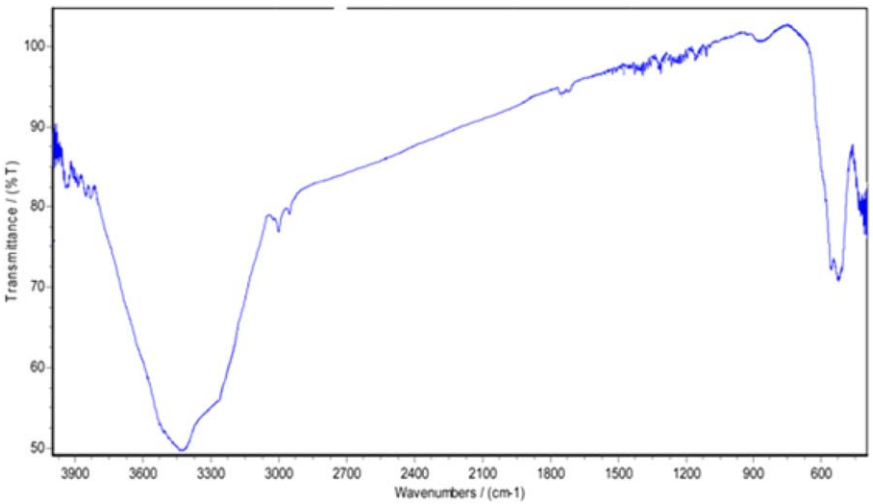

Figure 8. ATR-FTIR spectrum of coated-Fe_3O_4 nanoparticles.

[Color figure can be viewed at wileyonlinelibrary.com]

The ATR-FTIR pattern (Figure 8) for the sample shows broad bands at 580 and 400 cm^{-1} which is the characteristic of Fe_3O_4,[17,19] belonging to the stretch vibration mode and torsion vibration mode of Fe–O bonds in the metal tetrahedral and octahedral positions, respectively. An intense band appeared in the 3200–3600 cm^{-1} region can be attributed to the surface hydroxyl groups (O–H stretching vibration).[34] Moreover, the free O–H group adsorbed infrared radiation sharply at a frequency close to 3700 cm^{-1}. As can be seen in Figure 8, the adsorption of the O–H group that is no longer free is shifted to lower frequencies and become a broad band.

XRD analysis (Figure 9) was carried out to analyze the crystalline structure of the synthesized magnetite. It displays that the most intense reflections for the sample were in consistent with other literates.[30] Results confirm that the sample that has not been in contact with the TMAH from the very beginning but after alkalinizing with ammonia, has the low degree of crystallinity due to broad diffraction peaks and the noisy background.

Absortpion

The results in Figure 10 show that the average molar flux of carbon dioxide in nanofluid containing different nanoparticle mass fractions and molar flux of carbon dioxide in the base fluid containing different TMAH mass fractions. It indicated that the average molar flux obtained by Eq. 6 was increased by increasing the mass fraction of nanoparticles in the nanofluids, and it can be concluded that the addition of nanoparticles up to the maximum content of 1 wt % increased the molar flux to 2.8×10^{-5} mol/m^2 s and low amounts of nanoparticles could enhance mass transfer rate intensively. Furthermore, the results of this figure indicated that with the increase of TMAH in basefluid (deionized water) the absorption of CO_2 did not change declaring TMAH could not affect the mass transfer rate and the nanoparticles had major effect on the mass transfer enhancement.

Figure 11 shows the results of the average carbon dioxide absorption in nanofluids when exposed to AC and DC magnetic fields with different intesnies vs. rising bubble contact time (s) that was measured at the concentration of 1 wt % nanoparticles and a temperature of 25°C. These finding indicated that the absorption increased when the intensity of the field was increased and also the average molar flux decreased with an increase in contact time. The maximum absorption of CO_2 was occurred for AC magnetic field with intensity of 720 gausses and the absorption at different rising values of contact time for AC magnetic field with instensity of 350 gausses was approximately equal to the nanofluids exposed to the DC magnetic field which had the intensity of 720 gausses. These

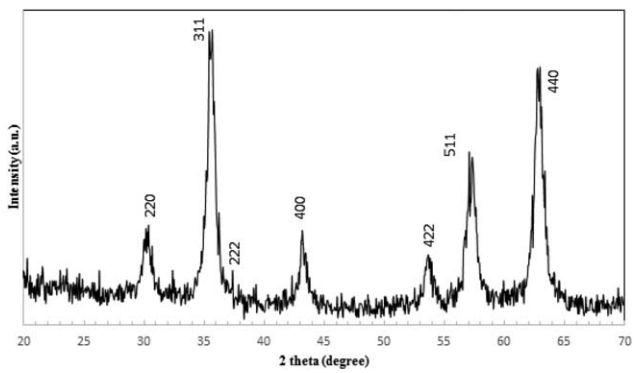

Figure 9. X-ray diffraction pattern for Fe_3O_4 magnetic nanoparticles.

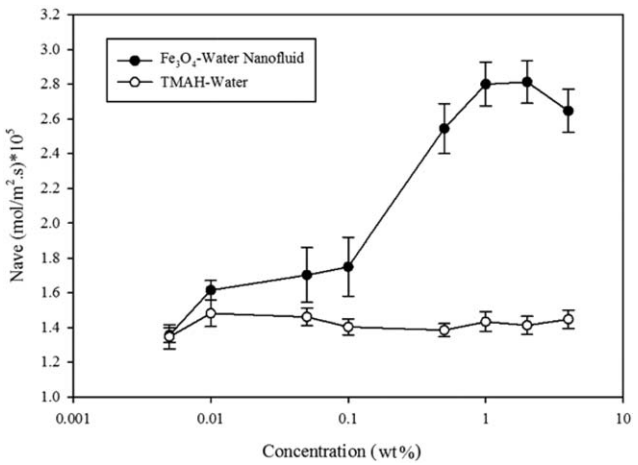

Figure 10. Average molar flux of carbon dioxide vs. nanoparticle mass fraction.

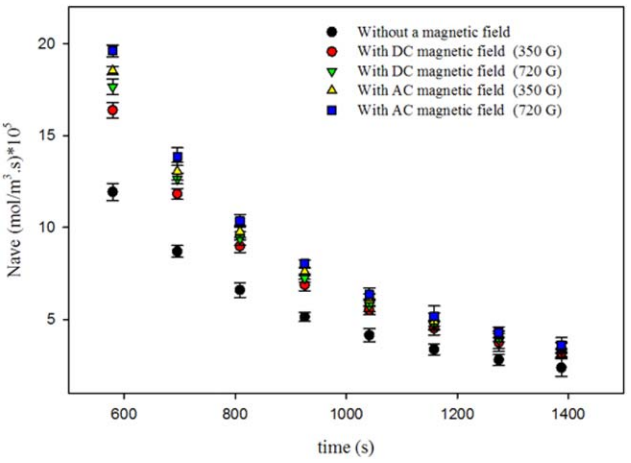

Figure 11. Average molar flux of carbon dioxide vs. rising bubble contact time.

[Color figure can be viewed at wileyonlinelibrary.com]

finding indicated that AC magnetic field which reversed its direction 50–60 times per second had major effect on mass transfer rate compared to static magnefic field. CO_2 absorption results for AC and DC electromagnetic fileds of different intensities are reported in Table 1.

It was appeared from the results that applying AC magnetic fields increased the mass transfer coefficient and consequently mass transfer rate more than DC magnetic fields in all experiments. The main mechanism for enhancing mass transfer rate was attributed to Brownian and random motions of nanoparticle under different external conditions. The increase in Brownian motion inducing micro convection caused higher mass transfer rate at liquid-gas interface. The magnitude of random motions of nanoparticles in basefluid are affected by applying magnetic field due to the magnetic properties of nanoparticles. Thus, AC magnetic field increases random motion of nanoparticles at liquid-gas interface resulting mass transfer coefficient enhancement.

Also as it is clear from Table 1, average molar flux of CO_2 into nanofluid for DC magnetic field had lower values compared to the Fe_3O_4/water magnetic nanofluid under the influence of AC magnetic fields. It can be attributed to the fact that during applying DC magnetic fields the formation of structure-chain-like aggregation in the samples occurred at liquid-gas interface. By formation of nanoparticles aggregation at gas-liquid interface due to the DC magnetic field, the Brownian motion of nanoparticles decreased and consequently the mass transfer coefficient for CO_2 absorption was reduced in comparison with AC magnetic field.

It should be noted that in all experiments, carbon dioxide was injected to nanofluids within volumes from 25 to 60 mL. Moreover, Gas-liquid contact time was calculated by multiplying number of bubbles by rising time of each bubble (3.76 s). Equation 8 indicates a gas-liquid mass transfer model for single bubble systems based on Dankwert's theory[23,26] applied to predict the gas-liquid mass transfer rate.

$$N_{\mathrm{av}}=\frac{D\ \sin h\left(\delta\sqrt{\frac{s}{D}}\right)+D\ r_0\ \sqrt{\frac{s}{D}}\ \cos h\left(\delta\sqrt{\frac{s}{D}}\right)}{r_0\ \sin h\left(\delta\sqrt{\frac{s}{D}}\right)}\left(C_{\mathrm{CO}_2,i}-C_{\mathrm{CO}_2}\right) \tag{8}$$

In this equation, the main factors influencing mass transfer rate are surface renewal rate (s), the bubble radius (r_0),

Table 1. Results of Carbon Dioxide Absorption Experimental Data Indicated by Titration for Fe_3O_4/Water Nanofluid Containing 1 wt % Fe_3O_4 Nanoparticles

Gas volume (mL)	Number of bubbles (n)	Gas-liq. Contact time $\theta = 3.76 \times n$ (s)	CO_2 concentration in liquid bulk From Eq. 5, (mol/m³)						Average molar flux, from Eq. 6, (mol/m² s) × 10⁵					
			Magnetic field type						Magnetic field type					
			AC (720 G)	AC (350 G)	No field	DC (350 G)	DC (720 G)		AC (720 G)	AC (350 G)	No field	DC (350 G)	DC (720 G)	
60	369	1387.44	26.08 ± 0.31	25.00 ± 0.33	17.2 ± 0.11	23.00 ± 0.31	24.00 ± 0.16		3.61 ± 0.40	3.46 ± 0.31	2.38 ± 0.49	3.19 ± 0.21	3.32 ± 0.40	
55	339	1274.64	26.20 ± 0.43	24.90 ± 0.26	17.1 ± 0.25	22.86 ± 0.22	23.80 ± 0.18		4.30 ± 0.28	4.08 ± 0.28	2.80 ± 0.30	3.75 ± 0.48	3.90 ± 0.48	
50	308	1158.08	26.10 ± 0.23	24.70 ± 0.43	17.0 ± 0.43	22.75 ± 0.13	23.65 ± 0.23		5.19 ± 0.55	4.91 ± 0.45	3.38 ± 0.29	4.52 ± 0.35	4.70 ± 0.25	
45	277	1041.52	25.90 ± 0.34	24.60 ± 0.23	16.9 ± 0.36	22.43 ± 0.25	23.53 ± 0.21		6.37 ± 0.34	6.05 ± 0.34	4.15 ± 0.36	5.51 ± 0.23	5.78 ± 0.33	
40	246	924.96	25.80 ± 0.67	24.40 ± 0.33	16.5 ± 0.68	22.10 ± 0.32	23.30 ± 0.22		8.04 ± 0.21	7.61 ± 0.21	5.14 ± 0.24	6.89 ± 0.31	7.26 ± 0.21	
35	215	808.40	25.40 ± 0.21	23.94 ± 0.34	16.2 ± 0.59	22.05 ± 0.43	23.05 ± 0.19		10.37 ± 0.34	9.77 ± 0.34	6.61 ± 0.40	9.00 ± 0.34	9.41 ± 0.34	
30	185	695.60	25.14 ± 0.11	23.70 ± 0.41	15.8 ± 0.32	21.46 ± 0.23	22.96 ± 0.15		13.86 ± 0.48	13.06 ± 0.48	8.71 ± 0.32	11.83 ± 0.29	12.65 ± 0.29	
25	154	579.04	24.65 ± 0.10	23.30 ± 0.30	15.0 ± 0.22	20.59 ± 0.22	22.19 ± 0.24		19.61 ± 0.32	18.54 ± 0.22	11.93 ± 0.46	16.38 ± 0.41	17.65 ± 0.42	

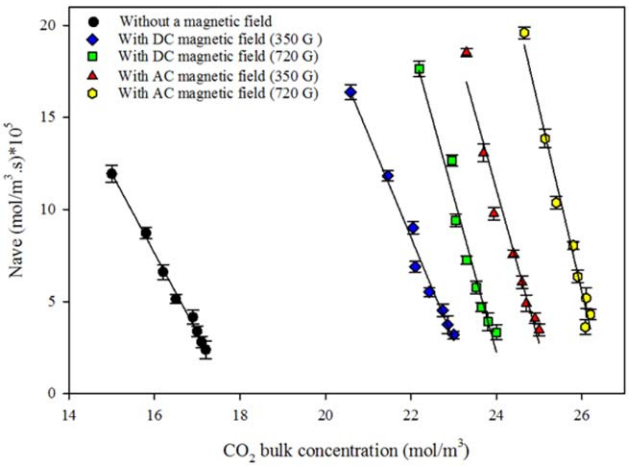

Figure 12. Average molar flux vs. concentration of carbon dioxide in liquid bulk and results of nonlinear multivariable regression based on Eq. 8.

[Color figure can be viewed at wileyonlinelibrary.com]

diffusion layer thickness (δ), and diffusion coefficient (D). N_{av} is mass transfer rate $\left(\frac{mol}{m^2}.s\right)$, C_{CO_2} is the bulk concentration of carbon dioxide in the liquid bulk (mol/m^3), and $C_{CO_2,i}$ is the concentration of CO_2 in the gas-liquid interface. Furthermore, Eq. 8 shows that gas concentration in the liquid phase at the gas-liquid interface (mol/m^3) that is equal to solubility of carbon dioxide in the liquid is independent of concentration and time[26] and can be obtained by contacting carbon dioxide and ferrofluid containing 1 wt % nanoparticles when exposed to magnetic fields for 24 h at ambient temperature (25°C) and total pure carbon dioxide pressure of 625 mm Hg. Then in this part carbon dioxide concentration in the bulk nanofluid, which is equal to the solubility of CO_2 in nanofluid, was measured by reversed titration.

The CO_2 concentration in the gas-liquid interface ($C_{CO_2,i}$), surface renewal rate (s), the bubble radius (r_0), diffusion layer thickness (δ), and diffusion coefficient (D) were predicted using multivariable nonlinear regression analysis on Eq. 8. To obtain model parameters, a regression with four independent variables performed by drawing a line that passes through the data points in a graph of molar flux vs. carbon dioxide concentration in liquid bulk (Figure 12). Curve fitting was done by using "curve fitting toolbar" in SPSS software version 22. The results of regression analysis are presented in Figure 12. These results showed that the regression analysis was performed with high accuracy and with the corresponding linear regression correlation coefficient value (R^2) equal to 0.96.

The theoretical solubility of CO_2 was compared with the values of experimental data obtained by contacting carbon dioxide with nanofluid containing 1 wt % Fe_3O_4 nanoparticles at various magnetic fields (Figure 13). It can be concluded from this figure that presence of nanoparticles led to increases in the solubility of carbon dioxide (has two polar C=O bonds) in nanofluids due to the existence of hydroxyl groups[17,35] and the enhancement of mass transfer due to grazing effect. In grazing effect, nanoparticles can increase the intensity of the fluid movement near the liquid-gas surface and particles move right through the concentration film layer and pick adsorbate up.[36] Moreover, these results exhibited the effects of magnetic field on CO_2 solubility. The increase in the intensity of magnetic field strength caused an increase in the solubility of carbon dioxide in the nanofluid. The validity of the model was verified by comparing the CO_2 concentration in the gas-liquid interface obtained through model and experimental data. These findings indicated that during absorption process in presence of AC external magnetic field solubility of CO_2 increases compared to the basefluid and is higher than those exposed to an DC magnetic field (Figure 13).

Mass transfer measurements demonstrated the enhancement of carbon dioxide solubility and the average molar flux gas into liquid phase, particularly in the case of AC magnetic field. This was attributed to the grazing effect and hydroxyl groups on nanoparticles' surfaces that the presence of magnetic field produced more grazing effect by making more particles to take part in this mechanism. In other words, the augmentation of the viscosity gradients and the Brownian motions in the absorption column resulted in increasing mass transfer.37 Figure 12 demonstrates that the enhancement of mass transfer caused by the increase in the magnetic field strength, partially in the case of AC magnetic field. This enhanced measurement confirms the positive effect of an external magnetic field, particularly in the case of AC magnetic field.

Diffusion layer thickness

According to Figure 14, results indicated significant changes in diffusion layer thickness in liquid regions that can be in consistent with results reported in other literature.[23,24] These results showed that with an increase in the magnetic field strength, the diffusion layer thickness decreased due to the increase in mass transfer rate. In the presence of AC magnetic fields that Fe_3O_4/water magnetic nanofluid showed better mass transfer enhancement, the diffusion layer thickness had lower values compared to the Fe_3O_4/water magnetic nanofluid under the influence of DC magnetic fields.

Renewal surface rate

Figure 15 shows the effect of magnetic fields on the renewal surface rate as a factor that claims the grazing effect. Other literature[24,38] has already applied the mechanical stirring or passage of a gas through suspend fine particles within a liquid and investigated the grazing effect. In this case, applying magnetic fields caused a significant increase in the renewal surface rate due to the decrease of the nanoparticles contact time with

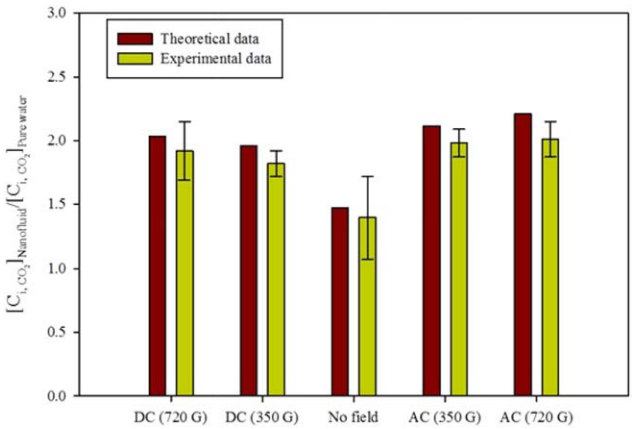

Figure 13. Relative concentration of CO_2 at gas-liquid interface for Fe_3O_4-water in the presense of AC and DC magnetic fields with different intensities.

[Color figure can be viewed at wileyonlinelibrary.com]

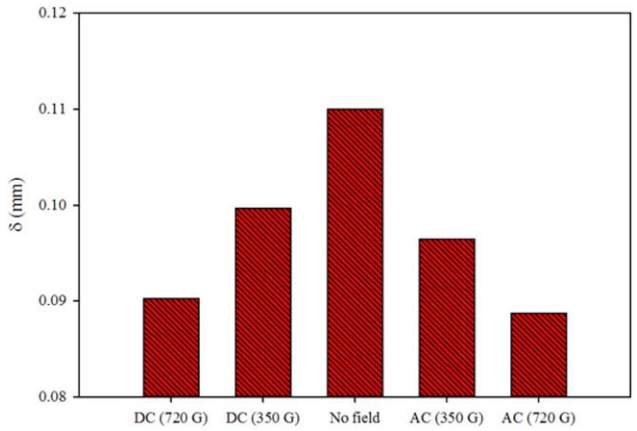

Figure 14. Diffusion layer thickness for carbon dioxide absorption into the Fe_3O_4-water in the presense of AC and DC magnetic fields with different intensities.

[Color figure can be viewed at wileyonlinelibrary.com]

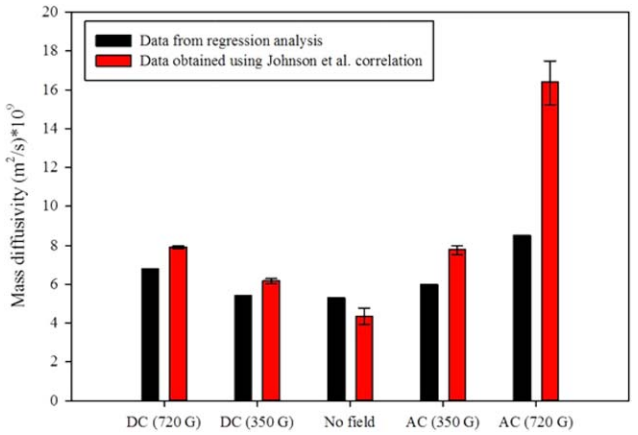

Figure 16. Diffusivity coefficient for carbon dioxide absorption in the Fe_3O_4-water in the presense of AC and DC magnetic fields with different intensities.

[Color figure can be viewed at wileyonlinelibrary.com]

bubble at gas-liquid interface as a result of physical effect of magnetic fields. This implies that this physical effect can be explained by the grazing effect. In other words, in such cases due to the fact that nanoparticles are smaller than film layer thickness of concentration boundary, these particles are able to adsorb the carbon dioxide in the film layer and then desorb them in the bulk liquid.[39,40] The magnetic field increases the mobility of nanoparticles resulting higher adsorption of carbon dioxide by means of nanoparticles at gas-liquid interface and desorption at bulk liquid. The AC 720 gausses magnetic field increases the renewal surface rate about three times higher than other magnetic field which is indicating the high mobility and microscopic random velocity of nanoparticles.

CO_2 diffusivity and nanofluid viscosity

The results of regression analysis for diffusivity at magnetic fields with different intensities are presented in Figure 16. The findings showed that by the increase in the magnetic field strength, diffusivity coefficient increased and AC magnetic field has more significant effect on diffusion coefficient compared to DC magnetic field. For comparison, a correlation (suggested by Johnson et al.) was used to calculate diffusivity coefficient for single rising bubble as follows[27]:

$$D=\left(\frac{0.45+0.2d_e}{U}\right)\left(\frac{K_{L,\ Experimental}}{1.13}\right)^2,\ 6\ mm < d_e < 40\ mm \tag{9}$$

Where d_e is equivalent spherical diameter of bubble (m), D is diffusivity of dissolved gas ($m^2\ s^{-1}$), U is bubble speed (ms^{-1}), and $K_{L,\ Experimental}$ is mass transfer coefficient ($K_{L,\ Experimental}=N_{av}/\left(C_{CO_2,i}-C_{CO_2}\right)$). The effect of magnetic field with different strength on diffusion coefficient was obtained using Eq. 9 for the Fe_3O_4-water nanofluid containing 1 wt % nanoparticles and also is presented in Figure 16. It confirmed that the diffusion coefficient increased with increased magnetic field strength. Because when the strength of magnetic field increased, more carbon dioxide could be transferred by means of nanoparticles that enhanced the gas component adsorption from the liquid film into the liquid bulk (shuttle mechanism).[23,33,36,37] Although the Eq. 9 can predict the diffusivity of CO_2 in Fe_3O_4 exposed to different magnetic fields, there is a large difference between the diffusivity calculated by regression analysis and ones calculated from Eq. 9. Because the mass transfer coefficient was just function of diffusion coefficient in Eq. 9 other parameters such as diffusion layer thickness and renewal surface rate could not be calculated using this equation; therefore, the values of diffusivity were more than those calculated using regression analysis. Therefore, it can be concluded that Eq. 9 could not be applied for absorption of gases with nanofluid in which grazing effect and also renewal surface rate may has important effect on mass transfer rate.

Even though according to Figure 17 the viscosity of Fe_3O_4-water nanofluid increased with an increase in the magnetic field strength, it might be assumed that diffusion coefficient decreased. However, other effects such as grazing effect, thermodynamic properties and Brownian diffusion might have affected this parameter. Furthermore, Figure 17 shows the increase in the viscosity of suspension induced by the external magnetic field and the additional of nanoparticles resulted in the enhancement of the mass transfer properties. This indicated that the effect of DC magnetic field induced more increase

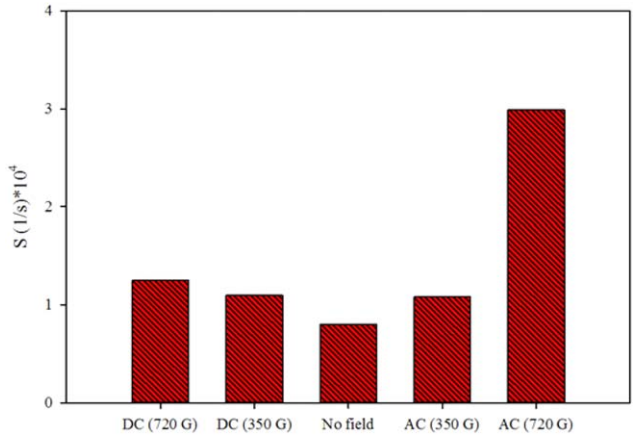

Figure 15. The surface renewal rates for carbon dioxide absorption in the Fe_3O_4-water nanofluid in the presense of AC and DC magnetic fields with different intensities.

[Color figure can be viewed at wileyonlinelibrary.com]

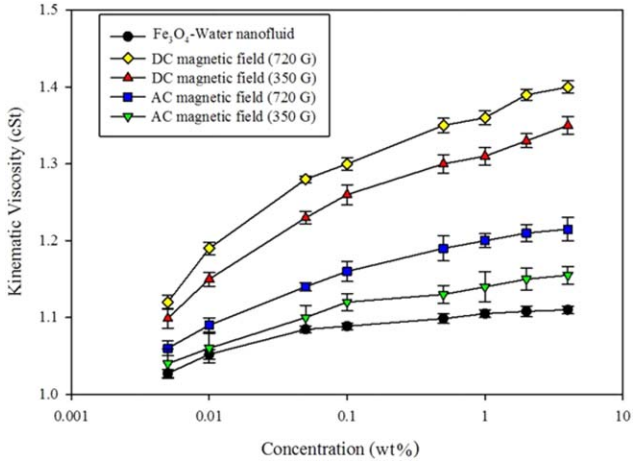

Figure 17. Kinetic viscosity of the Fe_3O_4-water nanofluid with different nano particles concentrations and different magnetic fields.

[Color figure can be viewed at wileyonlinelibrary.com]

in the viscosity that can be attributed to more particle migration and worm-like movements expected for nanoparticles.[41,42] Also these results showed that the viscosity of nanofluid increased with an increase in nanoparticles in the nanofluid.

According to the results of viscosity and diffusion coefficient of CO_2 in Fe_3O_4-water nanofluid at various magnetic fields, findings showed that the magnetic field reduced Schmidt number (for diffusion of CO_2 in pure water Sc is 410 at 300 K[43]) as a result of simultaneous increase in kinetic viscosity and diffusion coefficient (Figure 18). These results indicated that diffusivity of CO_2 in Fe_3O_4-water nanofluid was more than kinematic viscosity at various magnetic fields in comparison with pure water, and DC magnetic field has lower effect on diffusion coefficient due to the lower induced microcinvection resulting lower grazing effect at bubble surface.

Mass transfer coefficient

To investigate the validity of theoretical conclusion obtained through curve fitting of Eq. 8 on experimental data, mass transfer coefficient was calculated by two different methods. Equation 10 was applied to obtain theoretical mass transfer coefficient ($K_{L,\ Theoretical}$) by using calculated diffusion coefficient, diffusion layer thickness, and renewal surface rate

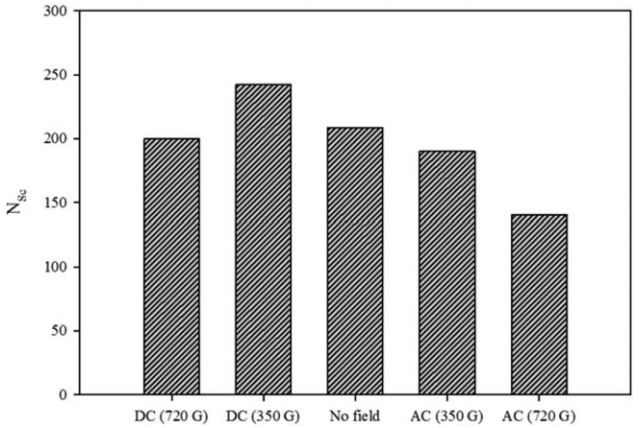

Figure 18. Schmidt number for CO_2 absorption using Fe_3O_4-water magnetic nanofluid in the presense of AC and DC magnetic fields with different intensities.

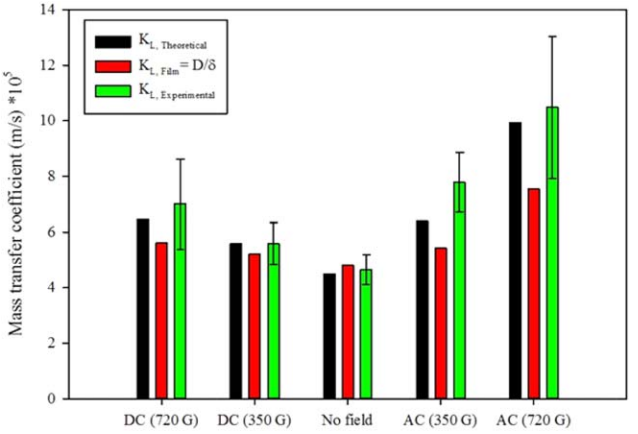

Figure 19. Average mass transfer coefficient exposed to different magnetic fields.

[Color figure can be viewed at wileyonlinelibrary.com]

from regression analysis. Then, the experimental mass transfer coefficient ($K_{L,\ Experimental}$) was calculated using average molar flux, CO_2 concentration at gas-liquid interface and liquid bulk ($K_{L,\ Experimental} = N_{av}/(C_{CO_2,i} - C_{CO_2})$).

$$K_{L,\ Theorectical} = \frac{D\ \sin h\left(\delta\sqrt{\frac{s}{D}}\right) + D\ r_0\ \sqrt{\frac{s}{D}}\ \cos h\left(\delta\sqrt{\frac{s}{D}}\right)}{r_0\ \sin h\left(\delta\sqrt{\frac{s}{D}}\right)} \quad (10)$$

Figure 19 shows experimental and theoretical mass transfer coefficients. These results showed that $k_{L,Theoretical}$ and $k_{L,\ Experimental}$ were same for each nanofuild in the presence of AC and DC magnetic fields with different intensities. Moreover, it can be concluded that the mass transfer coefficient of CO_2 absorption in Fe_3O_4-water nanofluid increased when the magnetic field was applied. These results showed that the nanofluid in the presence of AC magnetic field had higher mass transfer coefficient and for AC magnetic field with intensity of 350 gausses the mass transfer coefficient was similar for those exposed to DC magnetic field up to 720 gausses. To investigate the effect of renewal surface on mass transfer coefficient and mass transfer rate, $K_{L\ Film}$ was calculated by means of diffusion coefficient and diffusion layer thickness with 97% confidence in regression analysis. The results showed that with increased magnetic field strength, the deviation of film mass transfer coefficient ($K_{L\ Film}$) increased from experimental and theoretical mass transfer coefficients, it can be concluded that magnetic field increased the renewal surface rate due to intense grazing effect. The deviation of $K_{L\ Film}$ from experimental and theoretical mass transfer coefficient was much higher for an AC magnetic field which had an intensity of 720 gausses.

Conclusion

In this investigation, the absorption of carbon dioxide by using Fe_3O_4 magnetic nanoparticles with an average particle size of 10–13 nm synthesized using ferrous and ferric ions with $N(CH_3)_4OH$ was studied. The results of the average molar flux indicated a small change in the molar flux of surfactant-water system and a significant increase in the average molar flux by increasing the percentage of nanoparticles, due to incorporation of magnetic nanoparticles in the nanofluid. Mass transfer measurements indicated the enhancement of carbon dioxide solubility and the average molar flux, particularly in the case of alternative current magnetic field due to

grazing effects and the presence of hydroxyl groups on nanoparticles' surface. Diffusivity coefficient, liquid film thickness and renewal surface factor were calculated for the nanofluids exposed to external magnetic fields by means of a mathematical model. To validate the model, the results for experimental data have been compared with those obtained by theoretical conclusion. Finally, the results indicated that the effect of magnetic field on renewal surface rate caused unsatisfactory agreement between diffusion coefficient obtained from regression analysis and those obtained by other empirical correlation.

Acknowledgments

We thank our colleagues Iran Khorsandpour and Borzoo Karimi who provided insight and expertise that greatly assisted the research and also dr Nasrin Etesami faculty member of Isfahan University of Technology, Chemical Engineering Department, for her guidance during the research.

Literature Cited

1. Wu W, He Q, Chen H, Tang J, Nie L. Sonochemical synthesis, structure and magnetic properties of air-stable Fe_3O_4/Au nanoparticles. *Nanotechnology*. 2007;18(14):145609.
2. Abdollahi A, Salimpour MR, Etesami N. Experimental analysis of magnetic field effect on the pool boiling heat transfer of a ferrofluid. *Appl Therm Eng*. 2017;111:1101–1110.
3. Berger P, Adelman NB, Beckman KJ, Campbell DJ, Ellis AB, Lisensky GC. Preparation and properties of an aqueous ferrofluid. *J Chem Educ*. 1999;76(7):943.
4. Laurent S, Forge D, Port M, Roch A, Robic C, Vander Elst L, Muller RN. Magnetic iron oxide nanoparticles: synthesis, stabilization, vectorization, physicochemical characterizations, and biological applications. *Chem Rev*. 2008;108(6):2064–2110.
5. Chang W, Skandan G, Danforth SC, Kear B, Hahn H. Chemical vapor processing and applications for nanostructured ceramic powders and whiskers. *Nanostruct Mater*. 1994;4(5):507–520.
6. Akbarzadeh A, Samiei M, Davaran S. Magnetic nanoparticles: preparation, physical properties, and applications in biomedicine. *Nanoscale Res Lett*. 2012;7(1):144.
7. Tavakoli A, Sohrabi M, Kargari A. A review of methods for synthesis of nanostructured metals with emphasis on iron compounds. *Chem Pap*. 2007;61(3):151–170.
8. Turkdogan E, Olsson R, Vinters J. Gaseous reduction of iron oxides: part II. Pore characteristics of iron reduced from hematite in hydrogen. *Metall Mater Trans B*. 1971;2(11):3189–3196.
9. Petcharoen K, Sirivat A. Synthesis and characterization of magnetite nanoparticles via the chemical co-precipitation method. *Mater Sci Eng B*. 2012;177(5):421–427.
10. Gao X, Yu KK, Tam KY, Tsang SC. Colloidal stable silica encapsulated nano-magnetic composite as a novel bio-catalyst carrier. *Chem Commun*. 2003;(24):2998–2999.
11. Capek I. Preparation of metal nanoparticles in water-in-oil (w/o) microemulsions. *Adv Colloid Interface Sci*. 2004;110(1):49–74.
12. Huang X, Chen Z. Nickel ferrite on silica nanocomposites prepared by the sol–gel method. *J Magn Magn Mater*. 2004;280(1):37–43.
13. Borisenko VE, Gaponenko SV, Gurin V, Kam CH. *Physics, Chemistry and Applications of Nanostructures: Reviews and Short Notes*. Hackensack, NJ: World Scientific, 2011.
14. Janot R, Guérard D. One-step synthesis of maghemite nanometric powders by ball-milling. *J Alloys Compd*. 2002;333(1):302–307.
15. Teja AS, Koh P-Y. Synthesis, properties, and applications of magnetic iron oxide nanoparticles. *Prog Cryst Growth Charact Mater*. 2009;55(1):22–45.
16. Cheng F-Y, Su C-H, Yang Y-S, Yeh C-S, Tsai C-Y, Wu C-L, Wu M-T, Shieh D-B. Characterization of aqueous dispersions of Fe_3O_4 nanoparticles and their biomedical applications. *Biomaterials*. 2005; 26(7):729–738.
17. Andrade ÂL, Fabris JD, Ardisson JD, Valente MA, Ferreira JM. Effect of tetramethylammonium hydroxide on nucleation, surface modification and growth of magnetic nanoparticles. *J Nanomater*. 2012;2012:15.
18. Qu S, Yang H, Ren D, Kan S, Zou G, Li D, Li M. Magnetite nanoparticles prepared by precipitation from partially reduced ferric chloride aqueous solutions. *J Colloid Interface Sci*. 1999;215(1):190–192.
19. Andrade ÂL, Souza DM, Pereira MC, Fabris JD, Domingues RZ. pH effect on the synthesis of magnetite nanoparticles by the chemical reduction-precipitation method. *Quimica Nova*. 2010;33(3):524–527.
20. Vahedi A, Dehkordi AM, Fadaei F. Mass-transfer enhancement in single drop extraction in the presence of magnetic nanoparticles and magnetic field. *AIChE J*. 2015;62(12): 4466–4479.
21. Samadi Z, Haghshenasfard M, Moheb A. CO2 absorption using nanofluids in a wetted-wall column with external magnetic field. *Chem Eng Technol*. 2014;37(3):462–470.
22. Xuan Y. Conception for enhanced mass transport in binary nanofluids. *Heat Mass Transf*. 2009;46(2):277–279.
23. Esmaeili-Faraj SH, Nasr Esfahany M. Absorption of hydrogen sulfide and carbon dioxide in water based nanofluids. *Ind Eng Chem Res*. 2016;55(16):4682–4690.
24. Quicker G, Alper E, Deckwer WD. Effect of fine activated carbon particles on the rate of CO2 absorption. *AIChE J*. 1987;33(5):871–875.
25. Lopez JA, González F, Bonilla FA, Zambrano G, Gómez ME. Synthesis and characterization of Fe_3O_4 magnetic nanofluid. *Rev Latinoam Metal Mater*. 2010;30(1):60–66.
26. Zhao B, Wang J, Yang W, Jin Y. Gas–liquid mass transfer in slurry bubble systems: I. Mathematical modeling based on a single bubble mechanism. *Chem Eng J*. 2003;96(1):23–27.
27. Johnson A, Besik F, Hamielec A. Mass transfer from a single rising bubble. *Can J Chem Eng*. 1969;47(6):559–564.
28. Skoog DA, West DM, Holler FJ, Crouch SR. *Fundamentals of Analytical Chemistry*. Cengage Learning. 2013.
29. Teng T-P, Hung Y-H, Teng T-C, Mo H-E, Hsu H-G. The effect of alumina/water nanofluid particle size on thermal conductivity. *Appl Therm Eng*. 2010;30(14):2213–2218.
30. Vijayakumar R, Koltypin Y, Felner I, Gedanken A. Sonochemical synthesis and characterization of pure nanometer-sized Fe_3O_4 particles. *Mater Sci Eng A*. 2000;286(1):101–105.
31. Faraji M, Yamini Y, Rezaee M. Magnetic nanoparticles: synthesis, stabilization, functionalization, characterization, and applications. *J Iran Chem Soc*. 2010;7(1):1–37.
32. Darvanjooghi MHK, Esfahany MN. Experimental investigation of the effect of nanoparticle size on thermal conductivity of in-situ prepared silica–ethanol nanofluid. *Int Commun Heat Mass Transfer*. 2016;77:148–154.
33. Kim W-G, Kang HU, Jung K-M, Kim SH. Synthesis of silica nanofluid and application to CO2 absorption. *Sep Sci Technol*. 2008; 43(11–12):3036–3055.
34. Jahanbaani AR, Behzad T, Borhani S, Darvanjooghi MHK. Electrospinning of cellulose nanofibers mat for laminated epoxy composite production. *Fibers Polym*. 2016;17(9):1438–1448.
35. Davoodi SM, Sadeghi M, Naghsh M, Moheb A. Olefin–paraffin separation performance of polyimide Matrimid®/silica nanocomposite membranes. *RSC Adv*. 2016;6(28):23746–23759.
36. Kars R, Best R, Drinkenburg A. The sorption of propane in slurries of active carbon in water. *Chem Eng J*. 1979;17(2):201–210.
37. Esmaeili E, Ghazanfari R, Farsad S. Convective heat transfer enhancement of the water-based magnetite nanofluids in the presence of a 3-D low-intensity magnetic field. *Int J Nanodimens*. 2015;6(2):141.
38. Deckwer WD, Alper E. Katalytische suspensions-Reaktoren. *Chem Ing Tech*. 1980;52(3):219–228.
39. Kim J-K, Jung JY, Kang YT. The effect of nano-particles on the bubble absorption performance in a binary nanofluid. *Int J Refrig*. 2006;29(1):22–29.
40. Zhou M, Cai WF, Xu CJ. A new way of enhancing transport process – the hybrid process accompanied by ultrafine particles. *Korean J Chem Eng*. 2003;20(2):347–353.
41. Odenbach S, Thurm S. *Magnetoviscous Effects in Ferrofluids*. Berlin: Springer, 2002:185–201.
42. Shliomis MI, Morozov KI. Negative viscosity of ferrofluid under alternating magnetic field. *Phys Fluids*. 1994;6(8):2855–2861.
43. Treybal RE. *Mass-Transfer Operations*. 3rd ed., McGraw-Hill, New York, 1980.

Manuscript received July 21, 2016, and revision received Sep. 28, 2016.